

# LHCb Silicon Detectors: Operational Experience and Run I to Run II Transition

---

**Christian Elsasser**<sup>\*†</sup>

*Physik-Institut der Universität Zürich, Zurich, Switzerland*

*E-mail: [che@physik.uzh.ch](mailto:che@physik.uzh.ch)*

The main goals of the LHCb experiment are high-precision measurements of  $CP$  violation and searches for physics beyond the Standard Model with the high rate of beauty and charmed hadrons produced at the LHC. Essential prerequisites to perform such measurements are a detector with excellent impact parameter, vertex, and invariant mass resolution. This is achieved by the LHCb tracking system, in which several silicon detectors including the vertex locator surrounding the interaction region are deployed. This paper reports on the performance of the silicon detectors in the LHCb tracking system during the first data taking period of the LHC, describes the maintenance work done upon them in LHC Long Shutdown 1, and discusses possible challenges for the detectors in the LHC Run II.

*The 23rd International Workshop on Vertex Detectors*

*15-19 September 2014*

*Macha Lake, The Czech Republic*

---

<sup>\*</sup>Speaker.

<sup>†</sup>On behalf of the LHCb VELO and ST groups

## 1. Introduction

The LHCb experiment [1] is designed to study physics involving beauty and charmed hadrons in proton-proton collisions at the LHC. Since  $b\bar{b}$  and  $c\bar{c}$  pairs are predominantly produced with small polar angles with respect to the beam axis at the LHC, the LHCb detector is designed as a single-arm forward spectrometer covering the pseudorapidity range  $2 < \eta < 5$  ( $\eta = -\log(\tan \theta/2)$ ).

The LHCb tracking system consists of the Vertex Locator (VELO) surrounding the interaction region, a tracking station, called Tracker Turicensis (TT), upstream of a dipole magnet with a bending power of 4 Tm, and three tracking stations downstream of the dipole magnet. The inner part of these three stations is formed by the Inner Tracker (IT) while the outer part is covered by the Outer Tracker built as a straw tube detector. The VELO, the TT, and the IT are all silicon detectors and using silicon microstrip sensor technology.

## 2. The LHCb Silicon Detectors

### 2.1 The Vertex Locator (VELO)

The VELO consists of 42 modules arranged along the beam line, 21 on each side. They have the form of crescent-shaped half-disks and are built from two single-sided silicon microstrip sensors mounted back-to-back. While the sensor on one side measures the distance,  $r$ , from the beam axis, the sensor on the other side measures the azimuthal angle,  $\phi$ , of the position of charged particles traversing the module. During data taking the active part of the sensors is as close as 8 mm to the proton beams. Since this distance is much smaller than the aperture required for the beams during injection, the halves are retracted in the injection phase. Furthermore, the VELO modules are kept in a secondary beam vacuum, which is separated from the primary one by a 300  $\mu\text{m}$  thin undulated aluminum foil, shielding the modules from a possible pick-up of the radio frequency noise from the beam.

The VELO modules are made of  $n^+$ -on- $n$  doped silicon microstrip sensors (with the exception of the two most upstream modules, which use  $n^+$ -on- $p$  doped sensors) with a thickness of 300  $\mu\text{m}$ <sup>1</sup>. In the case of the  $r$ -sensors, they are divided into four 45°-quadrants and the strip pitch varies between 40  $\mu\text{m}$  (innermost radius) to 102  $\mu\text{m}$  (outermost radius). The  $\phi$ -sensors are segmented into two regions, an inner one and an outer one, with different stereo angles. These sensors have strip pitches between 38 and 101  $\mu\text{m}$ . The sensors are mounted on a carbon-covered substrate of Thermal Pyrolytic Graphite (TPG). The read-out strips are based on a double metal layer. The bottom layer forms the actual read-out strips while the top layer consists of the routing lines that guide the signal to the read-out electronics. This consists of 16 front-end Beetle chips [2] per sensor, located at the outer edge of the sensor. The sensor temperature during operation is about  $-10^\circ\text{C}$ .

### 2.2 The Tracker Turicensis (TT)

The TT consists of four planar detector layers made of 500  $\mu\text{m}$  thick  $p^+$ -on- $n$  doped silicon mi-

---

<sup>1</sup>The sensors were produced by Micron Semiconductor Ltd.

crostrip sensors<sup>2</sup>. The strip pitch of the sensors is 183  $\mu\text{m}$ . The strips in the first and last layers are aligned vertically. The strips in the central two layers are tilted by  $+5^\circ$  and  $-5^\circ$  in the second and third layers, respectively. The TT has an area of about 8  $\text{m}^2$  silicon in total. The sensors are grouped into read-out sectors consisting of one, two, three, or four sensors, which are bonded together. This leads to read-out strips with a length of up to 37 cm. The charge signals from the read-out strips are also processed by front-end Beetle chips. Their analogue output signal is then digitised and sent via optical fibres using VCSEL (vertical-cavity surface emitting laser) diodes to the counting house where the TELL1 [3] boards using FPGAs process the signals further. The detector is operated at a sensor temperature of 8°C.

### 2.3 The Inner Tracker (IT)

The IT is made of twelve detector layers (four in each tracking station downstream from the dipole magnet). The sensors are also  $\text{p}^+$ -on-n doped silicon microstrip sensors with a strip pitch of 198  $\mu\text{m}$ <sup>3</sup>. They are housed in four boxes per tracking station, one above and one below the beam pipe and one on each side of the beam pipe. Thus the IT presents a cross-like shape around the beam pipe. In the regions above and below the beam pipe each sensor corresponds to a read-out sector and has a thickness of 320  $\mu\text{m}$  while in the regions left and right of the beam pipe two sensors are bonded together to form a read-out sector. To ensure a large enough signal-to-noise ( $S/N$ ) ratio, the sensors have a thickness of 410  $\mu\text{m}$ . The read-out electronics chain for the IT is the same as for the TT and the sensors are also operated at a temperature of 8°C. The IT forms together with the TT the Silicon Tracker (ST).

## 3. Detector Performance

### 3.1 Signal-to-Noise Ratio

The signal-to-noise ratio is – in the case of the VELO – measured with the ADC counts of 1-strip clusters assigned to tracks reconstructed in the VELO and per strip common-mode subtracted noise. Figure 1(a) shows the distributions of the ADC counts for a  $\phi$ -sensor. It distinguishes the distributions from the read-out strips of the inner region and the outer region. In the case of the outer region, strips with and without a routing line on top are considered separately. Figure 1(b) shows the noise per strip in a  $\phi$ -sensor, where a significant increase in the noise is visible for strips with a routing line on top of themselves due to capacitive coupling. The obtained average  $S/N$  value for  $\phi$ -sensors is between 21 and 22 while it is between 18 and 20 for the  $r$ -sensors [4]. The dependence on the distance from the beam axis is shown in Fig. 2(a).

For the TT and the IT the  $S/N$  values were measured using clusters assigned to tracks with momentum  $p > 5 \text{ GeV}/c$ . The obtained values are between 12 and 15 for the TT and between 15 and 18 for the IT. Figure 2(b) displays the measured average  $S/N$  values for one-, two-, three-, and four-sensor read-out sectors in the TT as a function of the capacitance of the strips including cabling. It shows a linearly decreasing characteristic as a function of the channel capacitance.

<sup>2</sup>The sensors are identical in the design to the OB2 sensors used in the Outer Barrel of the CMS Silicon Tracker and were produced by Hamamatsu Photonics K.K.

<sup>3</sup>The sensors were designed and produced by Hamamatsu Photonics K.K.

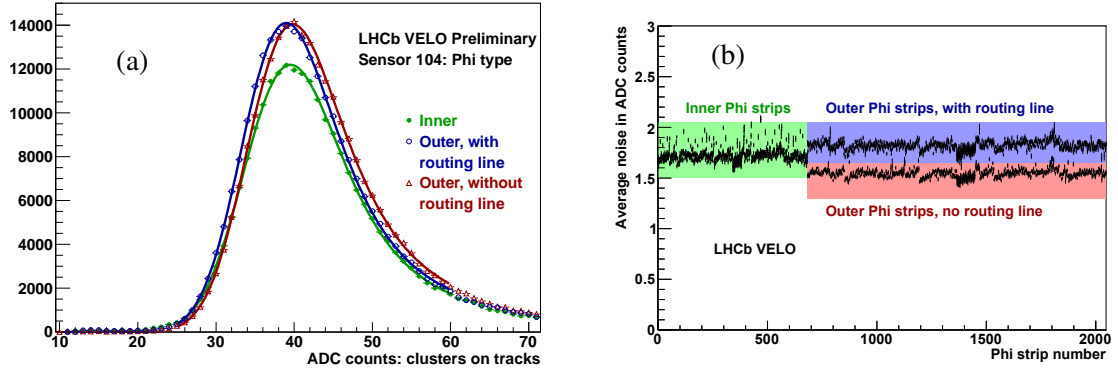


**Figure 1:** (a) ADC counts distributions in a  $\phi$ -sensor of the VELO distinguishing strips in the inner region and strips in the outer region with and without routing lines on top, (b) average noise per strip in a  $\phi$ -sensor where the bands show the standard deviation of the noise over all strips in  $\phi$ -sensors.

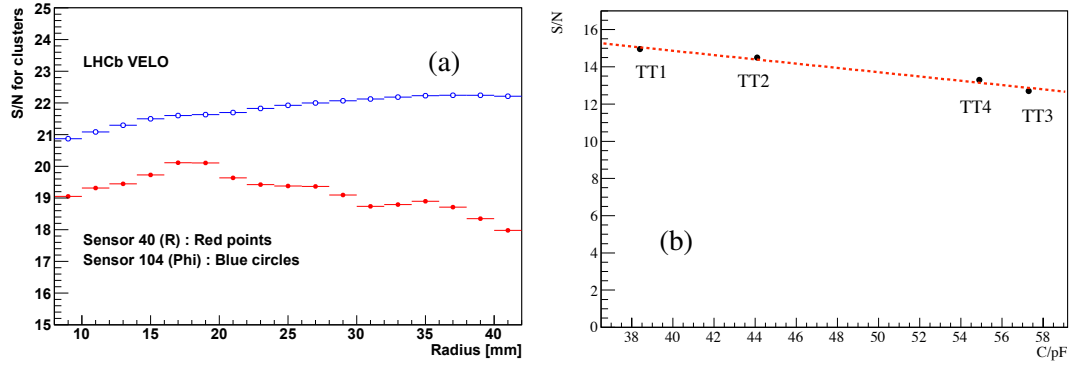


**Figure 2:** (a) Signal-to-noise ratio in the VELO sensors as a function of the distance from the beam axis, (b) average signal-to-noise ratio in the one-, two-, three-, and four-sensor (TT1-4) read-out sectors of the TT as a function of the channel capacitance.

### 3.2 Hit Resolution and Alignment

A crucial component for precise measurements by the tracking system is a good hit resolution as well as a precise alignment of the detectors. The hit resolution in the VELO depends on the strip pitch of the sensors and on the projected angles of the tracks<sup>4</sup>. As shown in Fig. 3(a), the hit resolution increases linearly with the strip pitch. Figure 3(b) displays the dependence of the hit resolution on the projected angle. The optimal projected angle for a given strip pitch corresponds to the situation in which the track crosses a width corresponding to the strip pitch while traversing the sensor. The best hit resolution achieved in the VELO is about 4  $\mu\text{m}$  for a minimal strip pitch and an ideal projected angle.

The alignment in the VELO was done during the production and installation phase with an

<sup>4</sup>The projected angle is the angle of the track with respect to the vertical on the sensor which is measured in the plane perpendicular to the read-out strips.

optical and mechanical survey leading to a high sensor position precision, *e.g.* the relative sensor position precision in  $x$  or  $y$  is  $3\ \mu\text{m}$ . The software alignment of the VELO is performed using the non-iterative Millipede method [5] based on matrix inversion and the minimisation of the track residuals from a Kalman filter fit [6]. The first method has the disadvantage of not incorporating multiple-scattering while the second one is CPU-time consuming in the case of large misalignment. The combined alignment precision for the VELO sensors is about  $4\ \mu\text{m}$  [4].

As the VELO is opened during injection and closed at the beginning of data taking, a centering of the two VELO halves with respect to the beam axis is performed based on the measured coordinates of the primary vertices separately measured by the two VELO halves. The difference in the measured coordinates between the two halves gives also an estimate of the alignment stability. In Run I the stability was about  $5\ \mu\text{m}$  in the  $x$ - and  $z$ -coordinates (*cf.* Fig. 4) and about  $3\ \mu\text{m}$  in the  $y$ -coordinate (*i.e.* in the vertical direction).

In the case of the TT and IT the alignment is done by minimising the track residuals from a Kalman filter fit [6]. Samples of  $J/\psi \rightarrow \mu^+\mu^-$  and  $D^0 \rightarrow K^-\pi^+$  candidates are used since they give vertex and mass constraints, which are beneficial to constrain weak modes [7]. Weak modes are degrees of freedoms in the alignment that are poorly constrained such as global scaling or rotations of the detector. Figure 5 shows the distributions of the unbiased track residuals for the TT and IT. They show a hit resolution including alignment effects of  $53.4\ \mu\text{m}$  in the TT and  $54.9\ \mu\text{m}$  in the IT compared to the binary resolution of the sensors of  $53$  and  $57\ \mu\text{m}$ , respectively.

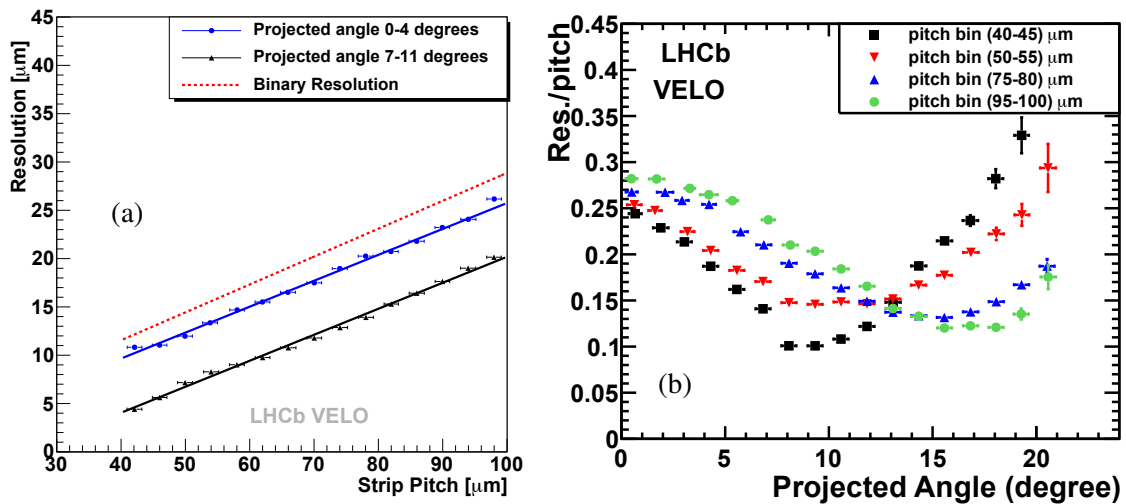


**Figure 3:** (a) Hit resolution in the VELO as a function of the strip pitch shown for two ranges of the projected angle and the benchmark from the binary resolution, (b) hit resolution relative to the strip pitch in the VELO as a function of the projected angle measured for different strip pitch ranges. The measurements are done using only 2-strip clusters.

#### 4. In-situ Monitoring of the Radiation Damage

The radiation damage monitoring is an important part in the prediction of the long term performance of silicon detectors. The type, the energy, and the flux of irradiating particles in LHCb

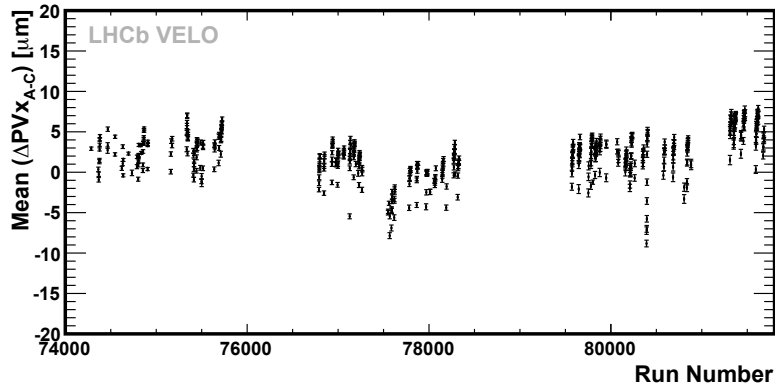


**Figure 4:** Measured difference in the  $x$ -coordinates of primary vertices reconstructed separately by the two VELO halves as a function of the run number (*i.e.* as a function of time) in 2010 data. The measured stability was about  $5 \mu\text{m}$ .

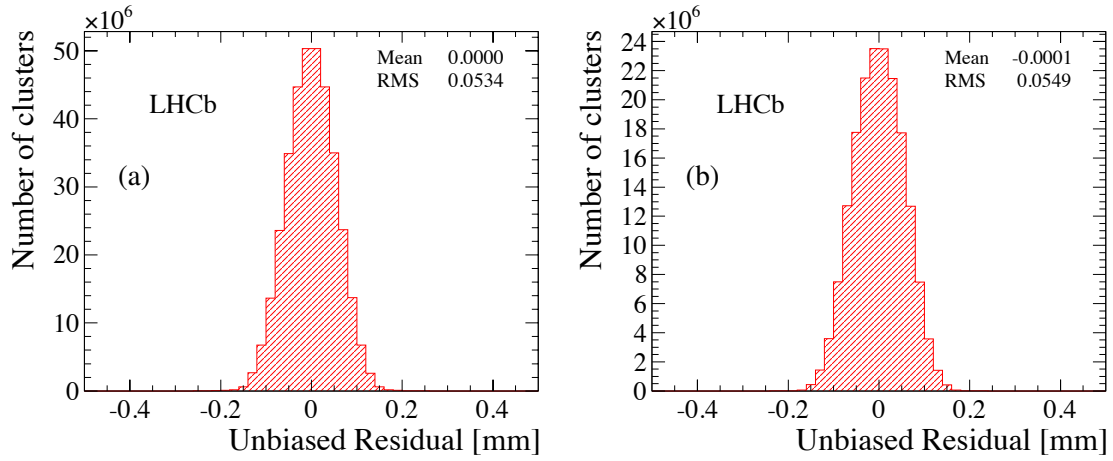


**Figure 5:** The distributions of track residuals for (a) the TT and (b) the IT in 2012 data. The hit resolution including alignment effect is estimated as the standard deviation of the distributions leading to a value of  $53.4 \mu\text{m}$  in the TT and of  $54.9 \mu\text{m}$  in the IT.

suggest that the dominating mechanism for radiation damage in the LHCb silicon detectors is non-ionising energy loss. There are mainly two methods applied to measure the radiation damage: On the one hand measurements of leakage currents are performed, and on the other hand the change in the depletion voltage of the sensors is monitored via dedicated Charge Collection Efficiency (CCE) scans.

#### 4.1 Leakage Current Measurements

As the irradiation in the LHCb silicon detectors causes predominantly bulk damage, it is expected that the observed change in the leakage current,  $\Delta I_{\text{leak}}$ , is proportional to the total particle fluence

$$\Delta I_{\text{leak}} = \alpha \cdot \Phi_{1 \text{ MeV-n,eq}} \cdot V_{\text{Si}}, \quad (4.1)$$

where  $\Phi_{1\text{ MeV-n,eq}}$  is the 1-MeV-neutron equivalent fluence,  $\alpha$  the corresponding damage factor, and  $V_{\text{Si}}$  the volume of the irradiated silicon.

The leakage currents are defined as the maximal currents measured per high voltage channel in each fill. Figure 6 shows the measured leakage currents as a function of time in the VELO and the IT. The currents in the IT are normalised to a sensor temperature of 8°C using the formula

$$\frac{I_{\text{leak}}(T_1)}{I_{\text{leak}}(T_2)} = \left(\frac{T_1}{T_2}\right)^2 \cdot \exp\left(\frac{E_g(T_1 - T_2)}{2k_B T_1 T_2}\right), \quad (4.2)$$

describing the temperature dependence of leakage currents induced by bulk damage (bulk currents) and where  $E_g$  is the band gap energy of silicon [8]. The measurements are compared with predictions of  $I_{\text{leak}}$  based on a FLUKA simulation [9] tuned with dose measurements in the LHCb cavern and incorporating annealing effects [10]. There is good agreement between measurements and predictions. The measured spread in  $I_{\text{leak}}$  reflects the difference in the fluence across the detectors. In the case of the VELO there are high-voltage channels showing much higher currents than predicted at a low irradiation of the sensors. This behaviour is attributed to a component in the leakage currents due to effects at the silicon-SiO<sub>2</sub> interface close to the surface of the sensors (surface currents). After irradiation corresponding to an integrated luminosity of about 0.5 fb<sup>-1</sup> this behaviour disappeared and all sensors were dominated by bulk currents. The contributions of bulk and surface currents to the leakage current were studied in the VELO with temperature-current scans since bulk currents have a temperature behaviour described by Eq. (4.2) while the surface currents are to first order independent of the sensor temperature [11].

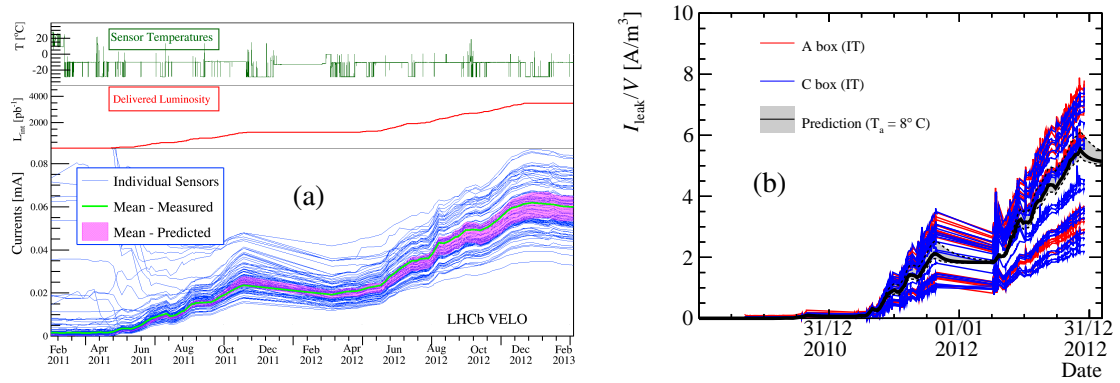


**Figure 6:** Measured leakage currents as a function of time in (a) the VELO and (b) the IT (shown for the detector boxes to the left and right of the beam pipe). The purple band in (a) and the black line and the grey band in (b) show the predicted leakage current evolution with uncertainties based on the mean particle flux in the considered sensors. The plots at the top of (a) show the average sensor temperature of the VELO sensors and the integrated delivered luminosity as a function of time.

#### 4.2 Depletion Voltage Measurements

The effective full-depletion voltage of the silicon sensors is monitored via dedicated CCE scans taking place three to four times a year. In these scans collision data are recorded for different

bias voltage settings in the VELO modules as well as in TT and IT detector layers. Since the bias voltage settings are not changed at the same time for all detector layers or modules, tracks from charged particles can still be reconstructed using the information from the detector elements operated at their nominal configuration. These tracks are used to estimate the position of the signal hits in the detector elements where the bias voltage is scanned. By summing up the ADC counts measured in the read-out strips surrounding this position, an unbiased ADC counts distribution is obtained (*cf.* Fig. 7(a)). The corresponding most probable value (MPV) is extracted from a fit of this distribution by a Landau distribution convolved with a distribution describing fluctuations of the ADC counts due to noise. Figure 7(b) shows the measured MPVs as a function of the applied sensor bias voltage for two VELO sensors.

Since the size of the depletion zone grows with the bias voltage, the MPV increases as a function of the bias voltage for small values. For large values the measured MPV saturates as the sensor is fully depleted. A spline function is fitted to the data, and the effective full-depletion voltage is estimated as the bias voltage where the spline function reaches a certain fraction of the saturation value (80 % in the VELO, 95 % in the ST). These fractions were calibrated by comparing the data from the first CCE scan with no irradiation and the measured depletion voltage after the sensor production [11].

Figure 8 shows the measured effective full-depletion voltage for the VELO and the TT as a function of the total 1-MeV-neutron equivalent fluence. Since the particle flux is largest for the region closest to the beam pipe, the progress in the depletion voltage evolution is also largest for sensors covering this region. The measured evolution of the depletion voltage is compared with predictions based on the Hamburg model [12]. The measurements and these predictions show good agreement for fluence values below  $10^{12} \text{ cm}^{-2}$  and in case of the VELO above  $2 \times 10^{13} \text{ cm}^{-2}$ . There is a disagreement between the measurements and the predictions for the VELO in the fluence range where the depletion voltage is predicted to drop to zero. This is most likely caused by the minimal electric field required in the sensor for the charge collection. Therefore the depletion voltage measurements in this region do not reproduce the actual depletion voltage of the sensors.

## 5. Work during Long Shutdown 1

As shown in the previous sections, the performance of all the three sub-detectors was very good, and no major change or repair work was required at the end of LHC Run I. Nevertheless, several interventions have been performed.

The largest intervention was the replacement of the chiller for the  $\text{C}_6\text{F}_{14}$  circuit in the TT and IT. During LHC Run I, a regular decrease – every two to three days – of the cooling power was observed, which was very likely caused by a contamination of the coolant by a lubricant of the chiller. The problem could be temporarily solved by recirculation of the coolant circuit. To solve this problem permanently a new chiller was installed and commissioned. Also the other parts (pumps, filters) of the cooling system as well as the biphasic- $\text{CO}_2$  cooling system of the VELO were maintained.

Further, maintenance of the VELO vacuum system and scheduled maintenance of the HV/LV supplies were done. Also broken parts of the DAQ and slow control electronics were replaced in

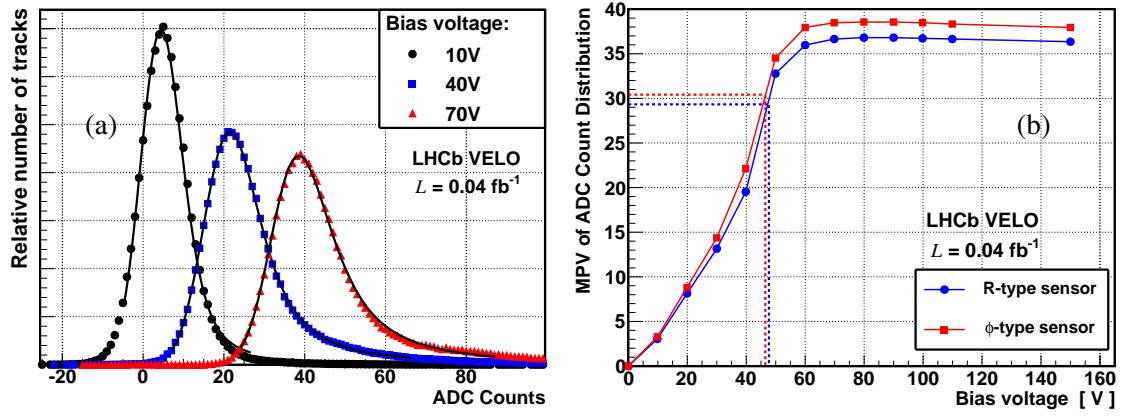


**Figure 7:** (a) ADC counts distributions in the VELO extracted from CCE scans for different bias voltage settings. The distributions are well described by a Landau distribution convolved with a Gaussian. (b) Measured MPV of the ADC counts distribution as a function of the applied bias voltage in an  $r$ - and a  $\phi$ -sensor. The dashed lines show the extraction of the effective full-depletion voltage values.

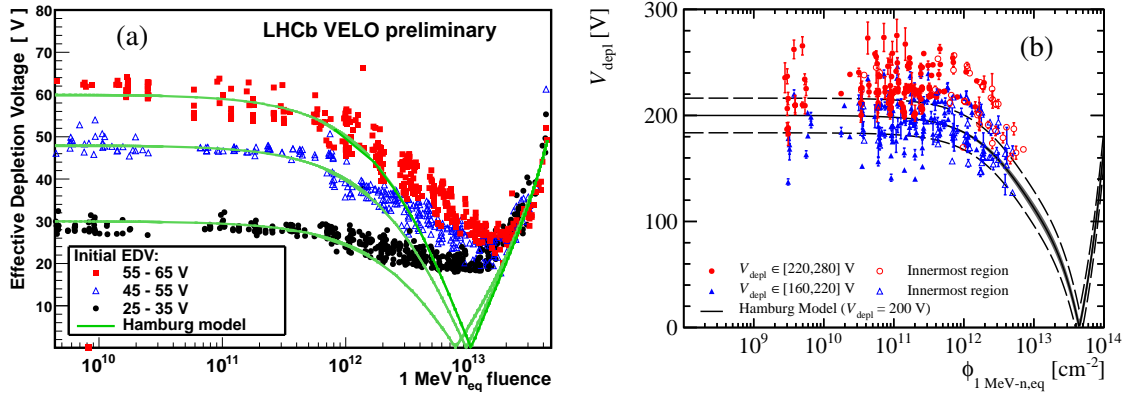


**Figure 8:** The effective full-depletion voltage values measured in the CCE scans as a function of the 1-MeV-neutron equivalent fluence for (a) the VELO and (b) the TT. The different colors of the data points show different ranges of the initial depletion voltage measured after production. The green lines in (a) and the black line in (b) show the predictions based on the stable damage part of the Hamburg model. The dashed lines in (b) show the average systematic uncertainty on the measurements.

the TT and IT. After these interventions the number of working channels is above 99 % in all three sub-detectors.

## 6. Summary and Conclusion

The silicon detectors of the LHCb experiment showed excellent performance during the first data taking period of the LHC. The monitoring of the radiation damage based on leakage current and depletion voltage measurements shows an evolution close to expectations. In the case of the VELO, the regions of the sensors closest to the beam axis are already in the regime of increasing depletion

voltage. Therefore modifications of the applied bias voltage in the LHC Run II with respect to Run I are required, and the details of the corresponding changes are under investigation. But expectations of the depletion voltage evolution show that the operation of the VELO will not be limited by radiation damage up to the end of Run II. Afterwards the VELO will be replaced in the upgrade of LHCb [13]. The extrapolated effect of the radiation damage in the TT and IT – also going to be replaced after Run II [14] – will not require any modification of the bias voltage settings in these detectors.

After standard maintenance work performed during the LHC Long Shutdown 1, the VELO, TT, and IT are ready for the data taking in Run II. Besides the higher centre-of-mass energy of up to 14 TeV in Run II, causing a higher occupancy, the LHC also aims for a short bunch-spacing of 25 ns. This might lead to higher rates of signal hits spilled over into the next bunch-crossing. The data acquisition and the data format of the signal hits were designed in anticipation of such effects. Further there are several studies ongoing to tune the parameters in the front-end electronics. This gives a faster signal pulse shape or a shift in the sampling time, which will allow the experiment to reduce the remainder of the signal pulse at the sampling point of the next bunch crossing (25 ns later) by trading it for a slightly lower signal-to-noise ratio.

## References

- [1] LHCb collaboration, A. A. Alves Jr. *et al.*, *The LHCb detector at the LHC*, *JINST* **3** (2008) S08005.
- [2] M. Agari *et al.*, *Beetle: A radiation hard readout chip for the LHCb experiment*, *Nucl. Instrum. Meth.* **A518** (2004) 468-469.
- [3] G. Haefeli *et al.*, *The LHCb DAQ interface board TELL1*, *Nucl. Instrum. Meth.* **A560** (2006) 494-502.
- [4] R. Aaij *et al.*, *Performance of the LHCb Vertex Locator*, *JINST* **9** (2014) P09007, [arXiv:1405.7808](https://arxiv.org/abs/1405.7808).
- [5] S. Viret, C. Parkes, and M. Gersabeck, *Alignment procedure of the LHCb Vertex Detector*, *Nucl. Instrum. Meth.* **A596** (2008) 157-163, [arXiv:0807.5067](https://arxiv.org/abs/0807.5067).
- [6] W. D. Hulsbergen, *The global covariance matrix of tracks fitted with a Kalman filter and an application in detector alignment*, *Nucl. Instrum. Meth.* **A600** (2009) 471 - 477.
- [7] J. Amoraal *et al.*, *Application of vertex and mass constraints in track-based alignment*, *Nucl. Instrum. Meth.* **A712** (2013) 48-55, [arXiv:1207.4756](https://arxiv.org/abs/1207.4756).
- [8] M. S. Sze and K. K. Ng, *Physics of Semiconductor Devices*, Wiley, 3rd ed., 2006.
- [9] A. Ferrari, P. R. Sala, A. Fasso, and J. Ranft, *FLUKA: A multi-particle transport code (Program version 2005)*, [CERN-2005-010](https://arxiv.org/abs/2005.010), [SLAC-R-773](https://arxiv.org/abs/SLAC-R-773), [INFN-TC-05-11](https://arxiv.org/abs/INFN-TC-05-11); G. Battistoni *et al.*, *The FLUKA code: Description and benchmarking*, *AIP Conf. Proc.* **896** (2007) 31-49.
- [10] CERN-ROSE/RD48 collaboration, M. Moll, E. Fretwurst, and G. Lindstrom, *Leakage current of hadron irradiated silicon detectors - material dependence*, *Nucl. Instrum. Meth.* **A426** (1999) 87-93.
- [11] A. Affolder *et al.*, *Radiation damage in the LHCb vertex locator*, *JINST* **8** (2013) P08002, [arXiv:1302.5259](https://arxiv.org/abs/1302.5259).
- [12] M. Moll, *Radiation damage in silicon particle detectors: Microscopic defects and macroscopic properties*, Ph.D. thesis, University of Hamburg, Dec. 1999, [DESY-THESIS-1999-040](https://arxiv.org/abs/DESY-THESIS-1999-040).

- [13] LHCb collaboration, *LHCb VELO Upgrade Technical Design Report*, [CERN-LHCC-2013-021](#), LHCb-TDR-013.
- [14] LHCb collaboration, *LHCb Tracker Upgrade Technical Design Report*, [CERN-LHCC-2014-001](#), LHCb-TDR-015.